Computational Electromagnetic Modelling of Compact Antenna Test Range Quiet Zone Probing: A Comparison of Simulation Techniques

C.G. Parini[1], R. Dubrovka[2], S.F. Gregson[3]
[1] Queen Mary University of London, London, UK, c.g.parini@qmul.ac.uk
[2] Queen Mary University of London, London, UK, r.dubrovka@qmul.ac.uk
[3] Nearfield Systems Inc. Torrance, CA, USA, sgregson@nearfield.com

***Abstract*—This paper extends the authors previous simulation study [1, 2] that predicted the quality of the pseudo plane wave of a single offset compact antenna test range (CATR). In this paper, the quiet-zone performance predictions are extended to rigorously incorporate the effects of probing the CATR quiet-zone using arbitrary but known field probes. This paper compares and contrasts results obtained using plane-wave-spectrum [3] and reaction integral [1, 3] based simulation techniques. This investigation leads to recommendations as to the optimal field probe choice and measurement uncertainties. The results of these new simulations are presented and discussed.**

***Index Terms*— Compact Antenna Test Range, Quiet-Zone Probing, Field-probe, Reaction Theorem, Plane Wave Spectrum.**

I. INTRODUCTION

The single-offset compact antenna test range (CATR) is a widely deployed measurement technique for the broadband characterization of electrically large antennas at reduced range lengths. The CATR collimates the quasi-spherical wave radiated by a low gain feed into a pseudo transverse electric and magnetic (TEM) plane-wave. The coupling of this locally plane-wave into the aperture of an antenna under test (AUT) creates the classical measured "far-field" pattern. The accuracy of an antenna measured using a CATR is therefore primarily determined by the uniformity of the amplitude and phase of this illuminating pseudo plane-wave [4].

Traditionally, the quality of the pseudo plane wave has been assessed by "probing" the amplitude and phase across a transverse planar surface with the results being tabulation on, typically, a plane-polar grid consisting of a series of linear scans in the horizontal, vertical and perhaps inter-carinal planes. A number of workers have utilized portable planar near-field antenna test systems to acquire two-dimensional plane-rectilinear data sets that can be used to provide far greater insight into the behaviour of the field in the quiet-zone (QZ) and additionally for the purposes of chamber imaging to provide angular image maps of reflections [5]. However, when mapping the CATR QZ the finitely large aperture of any realized field probe will inevitably affect the mapped fields by way of the convolution process between the pseudo plane wave of the CATR and the aperture illumination function of the scanning near-field probe, *cf.* [3]. Potentially, such a discrepancy can lead to confusion when comparing CATR QZ predications obtained from standard computational electromagnetic (CEM) models and empirical measurements as this "boxcar" field averaging process is not automatically incorporated within the numerical simulation. Several authors have undertaken CATR performance prediction modelling [4, 6, 7] with increasing levels of complexity. This paper extends our recently published comprehensive CATR QZ performance prediction software tool [1, 2] to incorporate the directive properties of several commonly used field probes so that recommendations can be made as to the most appropriate probe to use as well as providing estimates for the upper bound measurement uncertainty.

II. CATR QZ SIMULATION

The field illuminating the CATR offset parabolic reflector is typically derived from the assumed known far-field pattern of the feed antenna. This pattern could be derived from CEM simulation, as is the case here, or from empirical range measurements. Figure 1 contains a mechanical drawing of the WR430 choked cylindrical waveguide feed that was used during these simulations with the realised feed shown in Figure 2. Here, the feed is assumed nominally vertically polarised within its local coordinate system. When computing CATR QZ simulations for a horizontally polarised feed a vector isometric rotation [3, 4] can be used to rotate the probe by 90° about its local z-axis so as to produce equivalent far-field patterns for a horizontally polarised probe.

Figure 3 and 4 respectively illustrate the far-field amplitude and phase cardinal and inter-cardinal cuts of the feed antenna when resolved onto a Ludwig III co-polar and cross-pol polarisation basis [4]. These patterns were obtained from a proprietary three-dimensional full-wave CEM solver that used the finite difference time domain (FDTD) method.

The location of the phase centre was determined by means of a best-fit parabolic function over the $-50° \le \theta \le 50°$ angular range [5]. The maximum polar angle of 50° was selected as this is the maximum angle subtended at the feed by the CATR parabolic reflector. For angles larger than this, the feed pattern spills over from the reflector and the feed pattern function for angles larger than this are unimportant.

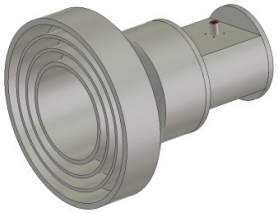

Fig. 1. Mechanical model of WR430 caTR feed.

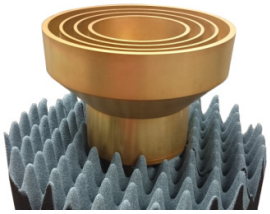

Fig. 2. Realised WR430 CATR feed.

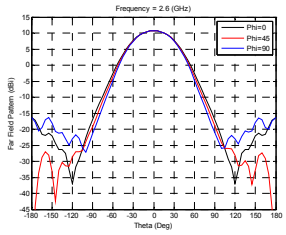

Fig. 3. Far-field Copolar amplitude cuts of feed at 2.6 GHz

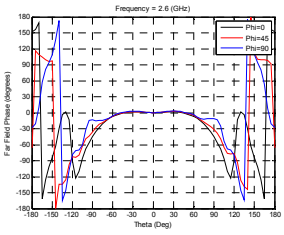

Fig. 4. Far-field copolar phase cuts of feed at 2.6 GHz

Here, the phase centre of this circular feed was determined as being at $x = y = 0$ m and z =-0.1377 m and was found to be extremely stable across the operating bandwidth. The phase patterns were compensated for this parabolic phase function, which conceptually corresponds to installing the phase centre of the feed at the focus of the CATR parabolic reflector. The field illuminating the parabolic reflector can then be determined from far-field antenna pattern function by reintroducing the (conventionally suppressed) spherical phase function and the inverse r term. The corresponding magnetic field, as required by the field propagation algorithm, can be computed from the electric field from the TEM far-field condition [4].

As a result of the requirement to minimise feed induced blockage, as described in [1, 2] a single offset reflector CATR design is harnessed. Here, it is assumed that the vertex of the reflector paraboloid is coincident with the bottom edge of the main reflector. Thus, the feed is required to be tilted up in elevation so that the boresight direction of the feed is orientated towards the centre of the reflector surface. In this case, the CATR main reflector is formed from an offset parabolic reflector with a focal length of 12' = 3.6576 m.

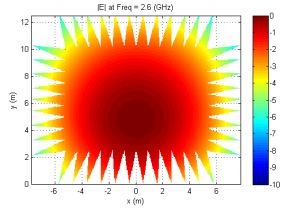

Fig. 5. Magnitude of illuminating electric field

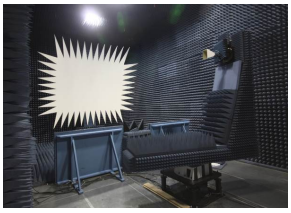

Fig. 6. Realized CATR reflector.

Figure 5 shows a false-colour plot of the magnitude of the illuminating electric field as radiated by the WR430 feed. Here, the boresight direction of the feed is pointing through the geometric centre of the reflector which corresponds to an elevation tilt angle of approximately 28°. Although this is a non-optimum illumination angle, in actuality a larger elevation angles is used to improve the CATR QZ amplitude taper by compensating for the spherical loss factor, 28°was used for the sake of consistency with prior simulations [1, 2]. Within Figure 5, the white space corresponds to regions where the reflectivity of the reflector is zero. Figure 6 shows an image of the reflector once installed within the test chamber.

The current element method [1, 2, 8] replaces fields with an equivalent surface current density $\underline{J}_s$ which is used as an equivalent source to the original fields. The surface current density across the surface of the reflector can be obtained from the incident magnetic fields and the surface unit normal using,

$$\underline{J}_s = 2\hat{\underline{n}} \times \underline{H}_i = 2\hat{\underline{n}} \times \underline{H}_r \tag{1}$$

The surface current density approximation for $\underline{J}_s$ (as embodied by the above expression) is known as the physical-optics approximation and allows for the computation of valid fields outside of the deep shadow region. The infinitesimal fields radiated by an electric current element can be obtained from the vector potential and the free-space Green's function [1, 8],

$$d\underline{H}(P) = \frac{da}{4\pi} \underline{J}_s \times \nabla\psi \tag{2}$$

This is an exact equation. When the field point is more than a few wavelengths from the radiating elemental source, the corresponding elemental electric fields can be obtained conveniently from the elemental magnetic fields using the far-field TEM condition using,

$$d\underline{E} = Z_0 \left(d\underline{H} \times \hat{\underline{u}} \right) \tag{3}$$

Thus, both the electric and magnetic fields can be obtained from the elemental fields by integrating across the surface of the parabolic reflector. In practice, for the case of a CATR with a QZ located at a distance z that is larger than the focal length of the reflector, the difference between the electric field as computed using the TEM condition and the exact formula is typically on the order of the limit of double precision arithmetic with this error being negligible. Figures 7 and 8 contain respectively false colour plots of the amplitude and phase patterns of the horizontally polarised electric field components of the pseudo-plane wave over the surface of a transverse plane located down-range at $z = 1.8f$ where f is the focal length of the CATR reflector. Figures 7, 8, 9 and 10 contain the E_x and E_y polarised amplitude and phase patterns for the horizontally polarised feed case. Although not shown, the equivalent magnetic fields were also computed. When interpreting these plots it is important to recognise that these are the fields one would measure if an infinitesimal electric (*i.e.* Hertzian) dipole probe were used to sample the QZ fields [3, 4]. This is in agreement with theory and standard CEM modelling tools. In practice, it is not possible to use an infinitesimal current element as a field probe and the following section examines how these patterns can be modified to

include the effects of an finitely large, *i.e.* directive, field probe.

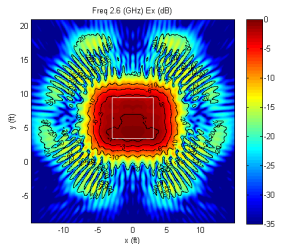

Fig. 7. Ex polarized QZ electric field amplitude.

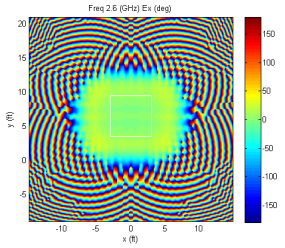

Fig. 8. Ex polarised QZ electric field phase.

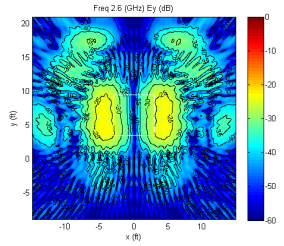

Fig. 9. Ey polarized QZ electric field amplitude

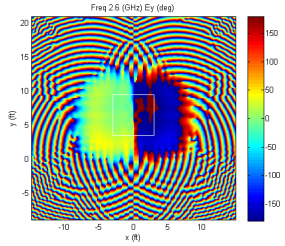

Fig. 10. Ey polarized QZ electric field phase

III. CATR QZ Probibng Simulation using Reaction Integral based Method

CATR QZ probing is usually accomplished by translating a field probe across a plane that is transverse to the z-axis of the CATR at several positions down-range. An example of a CATR QZ field probe can be seen presented in Figure 11. Here, the electrically small field probe can be seen positioned at the limit of travel of the 6' linear translation stage. Generally, pyramidal horns, *e.g. circa* 16 dBi standard gain horns (SGH) [4, 6], are used as CATR QZ probes as they have excellent polarisation purity, are easy to align, have some gain and therefore provide some immunity from reflections from the side and back walls of the anechoic chamber. An alternative choice of field probe is a *circa* 6 dBi gain open-ended rectangular waveguide probe (OEWG) [4].

Each of these field probes satisfy the primary requirements for a probe. These are, 1) time invariant gain and mechanical rigidity, 2) no pattern nulls in the forward hemisphere corresponding to a low directivity (as pattern nulls correspond to angles in which the probe is insensitive, i.e. blind, to incoming fields), 3) wide bandwidth minimising the necessity to use a multitude of probes to span a frequency range, 4) low scattering cross-section and reflection coefficient – i.e. well matched with a small return loss (to minimise the magnitude of the multiple reflections that are set up between the near-field probe and the AUT), 5) good polarisation purity, 6) good front to back ratio (so as to minimise sensitivity to probe placing and multiple reflections).

The probe used in CATR quiet-zone scanning procedure is itself an antenna and as such has its own antenna pattern. This has the effect of contributing a systematic error in the form of a singular mapping on top of the actual pseudo plane-wave generated by the CATR.

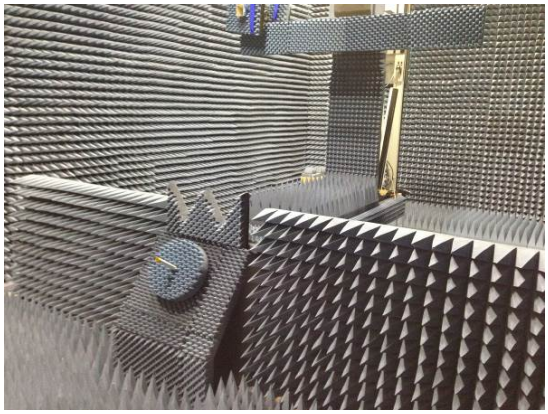

Fig. 11. CATR QZ field being probed using a linear translation stage mounted on AUT positioner uging a plane-polar acquisition scheme.

Thus the measured data is in fact the convolution of the CATR and probe responses. Furthermore, the clear difference in the electrical size of aperture of these two antennas and their directive properties and spatial filtering can be expected to result in some differences being observed between the probe measured QZ fields with the effects being quantifiable through an application of the reaction theorem which is a well-known method for analyzing general coupling problems [3]. This theorem states that, provided the electric and magnetic field vectors ($\underline{E}_1$, $\underline{H}_1$) and ($\underline{E}_2$, $\underline{H}_2$) are of the same frequency and are monochromatic, then the mutual impedance, Z_{21}, between two radiators, *i.e.* antennas 1 and 2, in the environment described by ε, μ can be expressed in terms of a surface integration [3],

$$Z_{21} = \frac{V_{21}}{I_{11}} = -\frac{1}{I_{11} I_{22}} \int_{S_2} \left(\underline{E}_2 \times \underline{H}_1 - \underline{E}_1 \times \underline{H}_2 \right) \cdot \hat{\underline{n}} \, ds \qquad (4)$$

Here, $\underline{n}$ is taken to denote the outward pointing surface unit normal. The subscript 1 denotes parameters associated with antenna 1 whilst the subscript 2 denotes quantities associated with antenna 2, where the surface of integration encloses antenna 2, but not antenna 1. Here, I_{11} is the terminal current of antenna 1 when it transmits and similarly, I_{22} is the terminal current of antenna 2 when it transmits. Note that this integral does *not* compute transferred power as there are no conjugates present and as such, crucially, phase information is preserved. Here, the fields $\underline{E}_1$ and $\underline{H}_1$ are used to denote the CATR QZ whilst fields $\underline{E}_2$ and $\underline{H}_2$ denote fields associated with the QZ field probe. From reciprocity, the mutual impedance, $Z_{12} = Z_{21}$, is related to the coupling between the two antennas. Clearly the mutual impedance will also be a function of the displacement between the antennas, their relative orientations, their directivities and their respective polarization properties. Once the impedance matrix is populated, this can be inverted to obtain the admittance matrix whereupon the required scattering matrix can be computed [3]. The elements $S_{1,2} = S_{2,1}$ of this two port scattering matrix are the complex transmission coefficients for the coupled antenna system which represent a

single point in the quiet-zone probing measurement. Although the integration can be performed across any convenient free-space closed surface, in this application integrating across the planar aperture of the OEWG or SGH antenna is perhaps the most computationally efficient strategy. Aperture fields can be obtained from analytical models [4] as in this case, from CEM simulation or from measurement with the choice being determined by the accuracy needed and the available information.

Figure 12 presents a comparison of the CATR QZ amplitude horizontal cut as obtained using an infinitesimal electric dipole (red trace) and an equivalent cut as obtained by using an OEWG probe (blue trace). A measure of the similarity between the respective measurements is provided by the equivalent multipath level (EMPL) [3] (magenta trace). From inspection of Figures 12 and 13, it is evident that the ideal (dipole) and OEWG measurements are in very good agreement, both in amplitude and phase for the horizontal cuts. This is further confirmed by the EMPL level that is at or below -60 dB right across the pattern peak, which corresponds to the useable QZ region.

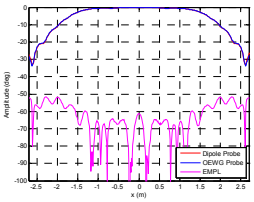

Fig. 12. Horizontal amplitude cut using dipole and OEWG field probe.

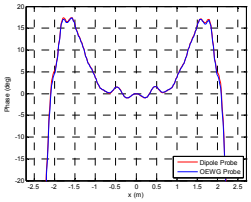

Fig. 13. Horizontal phase cut using dipole and OEWG field probe.

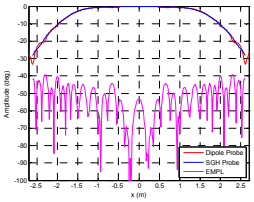

Fig. 14. Horizontal amplitude cut using dipole and SGH probe

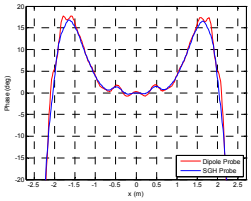

Fig. 15. Horizontal phase cut using dipole and SGH probe

Figures 14 and 15 contain equivalent figures for the case where a SGH has been used as a pyramidal horn probe. Here it is evident from inspection of the amplitude and phase results that the high spatial frequency information within the QZ plots has been attenuated with the larger aperture effectively averaging out the measured response and thereby reducing the observed amplitude and peak-to-peak phase ripple. This is further confirmed by the circa 15 dB increase in the EMPL level between dipole probe and horn probe. Although not shown due to lack of space, equivalent results for the vertical cut exhibited similar phenomena. This probe dependent QZ is a well-known measurement effect but for the first time it has been possible to bound the SGH upper-bound measurement uncertainty and to provide tools necessary for verifying the appropriate choice of field probes.

IV. CATR QZ Probibng Simulation using Plane Wave Spectrum based Method

An alternative way to compute the coupling between two antennas is to use the planar transmission formula that forms the basis of conventional planar near-field antenna measurement method [3, 9]. Ordinarily, the planar transmission formula is inverted to enable the fields transmitted by the antenna under test (AUT) to be compensated for the properties of the scanning near-field probe. Here, the converse operation is utilised. That is to say in this case the CATR is considered to be the "antenna under test" and this pattern is convolved with that of the field probe, which in this case is represented by either the OEWG probe or the SGH. This can be expressed in matrix form as [3],

$$[S] = \frac{j}{\lambda}[P]\cdot[M]\cdot[A] \tag{5}$$

Here, S denotes the received probe plane-wave spectrum (PWS), P contains the probe 'B' and 'C' angular spectrum, M the coordinate transformation and A the AUT plane wave spectral components where in this case the AUT comprises the offset reflector CATR. The relationship between the conjugate spatial and spectral quantities can be expressed in terms of a Fourier transform as [3, 4],

$$\underline{F_T}(k_x, k_y, z=0) = \int_{-\infty}^{\infty}\int_{-\infty}^{\infty} \underline{E_T}(x, y, z=0) e^{j(k_x x + k_y y)} dxdy \tag{6}$$

Conversely, the propagating electric field everywhere in the forward half space can be obtained from the tangential angular spectra as, [3, 4],

$$\underline{E_T}(x, y, z) = \frac{1}{4\pi^2}\int_{-\infty}^{\infty}\int_{-\infty}^{\infty} \left[\underline{F_T}(k_x, k_y)\right] e^{-j(k_x x + k_y y + k_z z)} dk_x dk_y \tag{7}$$

Thus, equation (6) can be used to compute the CATR QZ angular spectrum, equation (5) can be used to compute the coupling product, and equation (7) can be used to obtain the probed CATR quiet-zone fields. As only propagating field are considered, as we may assume that the quiet-zone is more than a few wavelengths from the CATR reflector then the limits of integration may be collapsed so that only homogeneous plane wave mode coefficients are considered where $k_x^2 + k_y^2 \le k_0^2$.

Hence, providing the CATR quiet-zone fields are not too truncated so that resulting spectral leakage in the spectral domain does not disturb the processed results too greatly, *cf.* [3], then the simulated probed fields can be computed efficiently and compared directly with those acquired either during a CATR QZ field-measurement or with those results presented in the preceding section. In general, we are free to compute our CATR quiet-zone over a plane of any finite extent and so in principal truncation is not a limiting factor. However, if for the purposes of efficiency the extent of the sampling plane is reduced then windowing techniques can be utilised to successfully compensate for this [3] providing only that some small degree of over-scanning is permissible.

Thus, by harnessing the PWS method set-out above CATR QZ results that are equivalent to those presented within the previous section were obtained. Figure 16 contains an equivalent plot only here the coupling was computed using the alternative PWS method. As can be seen the plots shown in Figure 16 and 14 are very similar with even the EMPL traces being in very close agreement. Figure 15 contains a comparison of the CATR QZ phase plot for the case where an infinitesimal Hertzian dipole probe is used, red trace, and a SGH, blue trace. Here, the coupling was computed using the reaction integral method.

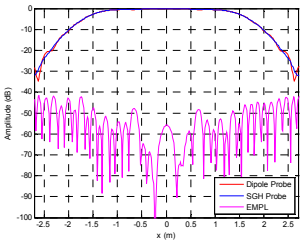

Fig. 16. PWS Method: Horizontal amplitude cut using dipole and SGH probe.

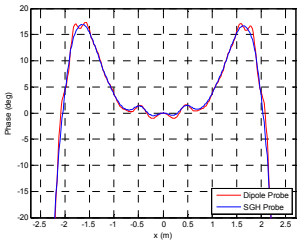

Fig. 17. PWS Method: Horizontal phase cut using dipole and SGH probe.

Again it is clear from inspection of these plots that the high spatial frequency ripple that is evident in the Hertzian dipole probed fields is largely absent from the SGH field probe simulation. This is in close agreement with what is found in practice and lends further confidence to the reliability of the method. Figure 17 contains an equivalent phase plot only here the PWS method was used to compute the coupling. Again the agreement that is attained between the respective phase plots, *i.e.*, Figures 15 and 17 is very encouraging as the same result is obtained when using entirely different simulation methodologies.

Although not shown as a consequence of available space, equivalent vertical cuts of the quiet-zone cuts were also simulated and the degree of agreement in amplitude and phase plots were similar.

V. Summary and Conclusions

This paper details the CEM simulation of the measurement of a CATR QZ using arbitrary but known near-field probes using two completely different simulation techniques. The verification of these simulation techniques is achieved through comparison of predicted results. Both the PWS based and reaction integral modelling techniques presented above comprise very general treatments of the CATR quiet-zone probing procedure. As such these include effects associated with cross polarisation and polarisation purity of the respective scanning field probes. An added benefit of the simulation techniques is that it is possible to utilise measured or simulated patterns for the field probe which further enhance the generality of the process. As an added benefit, the PWS coupling method also provides, inherently, the ability to simulate probed CATR QZ fields across a surface that is transverse to the range boresight direction at other z-axis positions down-range. This is by virtue of the differential phase change that can be applied to the plane wave spectra prior to performing the numerical integration to reconstruct the spatial field components.

References

[1] C.G. Parini, R. Dubrovka, S.F. Gregson, "CATR Quiet Zone Modelling and the Prediction of 'Measured' Radiation Pattern Errors: Comparison using a Variety of Electromagnetic Simulation Methods" AMTA October 2015.

[2] C.G. Parini, R. Dubrovka, S.F. Gregson, "Compact Range Quiet Zone Modelling: Quantitative Assessment using a Variety of Electromagnetic Simulation Methods", LAPC, November 2015.

[3] S.F. Gregson, C.G. Parini, J. McCormick, "Principles of Planar Near-Field Antenna Measurements", IET Press, 2007.

[4] C.G. Parini, S.F. Gregson, J. McCormick, D. Janse van Rensburg, "Theory and Practice of Modern Antenna Range Measurements", IET Press, 2014.

[5] G.E. Hindman, D. Slater, "Anechoic Chamber Diagnostic Imaging", AMTA Symposium 1992.

[6] M. Philippakis, C.G. Parini, "Compact antenna range performance evaluation using simulated pattern measurements", IEE Proceedings Microwaves, Antennas and Propagation, Volume: 143 , Issue: 3 DOI: 10.1049/ip-map:19960398, 1996, Page(s): 200 – 206.

[7] C.G. Parini, M. Philippakis, "The use of quiet zone prediction in the design of compact antenna test ranges", IEE Proc., Microwave Antennas Propagation, 1996, 143, (3), pp. 193-199

[8] A.D. Olver, P.J.B. Clarricoats, A.A. Kishk, L. Shafai, "Microwave Horns and Feeds", IEE Press, 1994.

[9] D. Kerns, "Plane-Wave Scattering-Matrix Theory of Antennas and Antenna-Antenna Interactions", NBS Monograph 162, 1981.